Published OnlineFirst December 6, 2010; DOI: 10.1158/0008-5472.CAN-10-0605

Cancer Research

High PTP4A3 Phosphatase Expression Correlates with Metastatic Risk in Uveal Melanoma Patients

Cécile Laurent[1,7,10,11,12,13], Fabien Valet[1,2,7,13], Nathalie Planque[1,8,10,11,12], Licia Silveri[1,3,10,11,12], Selma Maacha[1,10,11,12], Océane Anezo[1,10,11,12], Philippe Hupe[1,7,9,13], Corine Plancher[1,2], Cécile Reyes[1,3], Benoit Albaud[1,3], Audrey Rapinat[1,3], David Gentien[1,3], Jérôme Couturier[1,4], Xavier Sastre-Garau[1,4], Laurence Desjardins[1,5], Jean-Paul Thiery[14], Sergio Roman-Roman[1,3], Bernard Asselain[1,2,7,13], Emmanuel Barillot[1,7,13], Sophie Piperno-Neumann[1,6], and Simon Saule[1,10,11,12]

Abstract

A high percentage of uveal melanoma patients develop metastatic tumors predominantly in the liver. We studied the molecular profiles derived from gene expression microarrays and comparative genomic hybridization microarrays, to identify genes associated with metastasis in this aggressive cancer. We compared 28 uveal melanomas from patients who developed liver metastases within three years of enucleation with 35 tumors from patients without metastases or who developed metastases more than 3 years after enucleation. Protein tyrosine phosphatase type IV A member 3 (PTP4A3/PRL3), was identified as a strong predictor of metastasis occurrence. We demonstrated that the differential expression of this gene, which maps to 8q24.3, was not merely a consequence of 8q chromosome overrepresentation. *PTP4A3* overexpression in uveal melanoma cell lines significantly increased cell migration and invasiveness *in vivo*, suggesting a direct role for this protein in metastasis. Our findings suggest that PTP4A3 or its cellular substrates could constitute attractive therapeutic targets to treat metastatic uveal melanomas. *Cancer Res; 71(3); 666–74. ©2010 AACR.*

Introduction

Uveal melanoma is the most common intraocular cancer in adults. Up to 50% of patients develop metastases within a median of 36 months, with a median survival of 6 months after metastasis (1). Several clinical and histopathological features have been correlated with survival, including patient age (>60), anterior location of the tumor, tumor cell histology, largest diameter of the tumor, mitotic activity, and chromosome 3 monosomy. The most frequent chromosomal imbalances in uveal melanoma are loss of chromosome 3 and gains of 8q and 6p (2). Several gene expression profiling studies have identified two molecular classes strongly associated with metastatic risk (3–5). The application of one recently described gene classifier (6) to our data set (Supplementary Fig. 1) separates two classes, but 21% of metastasizing tumors remain associated with the low-grade group (class 1), justifying further analyses of gene expression to identify genes more specifically associated with metastasis.

We present here an analysis of gene expression in 63 primary tumors. The genes differentially expressed between *meta1* (patients who developed metastasis within 3 years of enucleation) and *meta0* (late- or nonmetastasizing tumors) tumors included a gene encoding protein tyrosine phosphatase type IV A member 3 (PTP4A3), which maps to 8q24.3. High levels of expression of this gene are highly predictive of metastasis. DNA copy number analysis has shown that 8q is overrepresented in high-risk tumors (2). However, the expression profile of *PTP4A3* differed considerably from that of the neighboring genes in the genome, demonstrating that this gene was not simply a passenger gene. We further investigated the role of *PTP4A3* in the development of tumor metastases, by characterizing the migration and invasiveness of uveal melanoma cell lines overexpressing this gene. Our results strongly suggest that the prognosis marker *PTP4A3* may play a causal role in metastasis development in uveal melanoma tumors.

Materials and Methods

Tumor samples and clinical data

A series of 63 tumor samples obtained by enucleation in untreated patients was provided by the Biological Resource Centre of Institut Curie. The study was approved by the ethics committee of Institut Curie and conformed to the Helsinki Declaration. In line with French regulations, informed consent was obtained from the patients concerned. Clinical,

Authors' Affiliations: [1]Institut Curie and Departments of [2]Biostatistics, [3]Translational Research, [4]Tumor Biology, [5]Ocular Oncology, and [6]Medical Oncology, Institut Curie; [7]INSERM, U900; [8]Univ Paris 7; [9]CNRS, UMR144, Paris, France; [10]Univ Paris-Sud 11; [11]CNRS, UMR3347; [12]INSERM, U1021, Orsay France; [13]Mines ParisTech, Fontainebleau, France; and [14]Translational Research, IMCB A*STAR, Singapore, Singapore

Note: Supplementary data for this article are available at Cancer Research Online (http://cancerres.aacrjournals.org/).

Corresponding Author: Simon Saule, Institut Curie UMR3347 CNRS, U1021 INSERM, Université Paris-Sud 11 Batiment 110, Centre Universitaire F-91405 Orsay, France. Phone: 33-1-69-86-71-53; Fax: 33-1-69-07-45-25; E-mail: simon.saule@curie.u-psud.fr

doi: 10.1158/0008-5472.CAN-10-0605

Published OnlineFirst December 6, 2010; DOI: 10.1158/0008-5472.CAN-10-0605

pathological, and molecular features of the tumors are presented in Supplementary Table 1.

We compared tumors displaying early and late or no metastasis (the *meta1* and *meta0* groups, respectively), by investigating patients with a minimum follow-up of 36 months, providing a subset of 57 cases. DNA copy number data were available for 45 of these patients (2). The others were assessed for chromosome 3 monosomy by FISH. Twenty-eight of these 57 patients developed liver metastasis in the first 36 months after diagnosis (*meta1* in our study), seven developed liver metastasis after 36 months and 22 had not developed liver metastasis at the time of analysis (noted *meta0*).

Expression microarray analysis

Labeled cRNA was produced from total RNA, and hybridization, scanning and image analysis were carried out as recommended by the manufacturer of the microarray (Affymetrix), with a two-round amplification protocol. Specimens were analyzed on GeneChip Human Genome U133 Plus 2.0 microarrays (Affymetrix). We used GeneChip Operating Software and the MAS 5.0 algorithm (Affymetrix) to control raw microarray data for the quality of hybridization and synthesis.

Analysis of gene expression data

The data set, corresponding to 63 uveal melanoma primary tumors, is available from the GEO database (http://www.ncbi.nlm.nih.gov/geo/), under accession number GSE22138. These data were analyzed with R software (version 2.9.0) and Bioconductor (release 2.4, refs. 7 and 8). Gene expression values for 63 uveal melanoma primary tumors were normalized with the GC-Robust Multi-array Average (GC-RMA) algorithm (9) and filtered, to remove probe sets with expression levels below 3.5 ($\log_2$ scale) in all samples.

Survival analysis on 63 patients

Univariate Cox models were first applied, to identify clinical variables (from Supplementary Table 1) significantly associated with the endpoint (metastasis-free survival). We then carried out stepwise multivariate Cox model analysis to identify, among these selected variables, a group of clinical variables significantly associated with the endpoint. Univariate and multivariate selections were based on Wald tests, with statistical significance fixed at 5%. The final multivariate model is referred to as the *clinical model*.

For additional filtering, we discarded half the probe sets displaying low levels of variability in expression levels: probe sets with interquartile range values (difference between the third and the first quartile) below the median value were removed. We then used univariate Cox models to detect probes significantly associated with the endpoint. We carried out Wald tests, with correction of the *P* values obtained as described by Benjamini and Hochberg, to account for multiple testing (10).

We investigated whether *PTP4A3* could be used to predict metastasis-free survival, by considering *PTP4A3* as a binary variable and distinguishing between patients with low and high levels of expression of this gene. We used the median level of expression as a threshold. The contribution of this binary variable to endpoint prediction was assessed with Wald tests in (i) the univariate Cox model and (ii) the multivariate Cox model adjusted for clinical parameters. These models are referred to as the *genomic*, and *clinical and genomic models*, respectively.

The predicted scores (fitted values) from these two models were used to identify groups of patients with significantly different prognoses. For the *clinical and genomic models*, we propose the use of the first and third quartiles to distinguish between patients with good, intermediate, and poor prognoses. For the *genomic model*, we propose the use of the median score threshold to distinguish between patients with good and poor prognoses. The median threshold for the genomic model was also validated on an external data set of 21 primary tumors (3). A log-rank test was used to compare the prognoses of the various groups defined by the models.

Gene expression analysis on the 57 primary tumors

We carried out a principal component analysis (PCA) on the tumor samples, based on the 12 discriminatory genes previously described (6). Because of differences between the platforms used, the mean value of the probe sets for the 12 published genes was used for the PCA.

Genes differentially expressed between the 29 *meta0* and the 28 *meta1* tumors were identified by the significance analysis of microarrays (SAM) method (11). The analysis parameter delta was fixed so as to give a false discovery rate (FDR) $\leq$5%. Genome-transcriptome correlation analysis (GTCA) was performed, by Pearson's correlation method, on 45 tumors for which both DNA copy number and RNA transcriptome information were available. We evaluated the correlation between the expression levels of neighboring genes along the genome, with the Transcriptome Correlation Map (TCM) method proposed by Reyal et al. (12). The correlation was calculated with a moving window of 20 genes around each gene.

Generation of OCM-1 cells stably producing EGFP-PTP4A3

Human OCM-1 uveal melanoma cells were obtained in 2003 from Dr. Frederic Mouriaux, (from ref. 13). These cells were analyzed for this study on GeneChip Human Genome U133 Plus 2.0 and Human Exon 1.0 ST Arrays (Affymetrix) and expressed MITF and the pigmentation genes. They were transfected with pEGFPc1 (Clontech) plasmids encoding the wild-type form of PTP4A3, the catalytic mutant C104S (both kindly provided by Prof. Qi Zeng, IMCB Institute, Singapore) or EGFP as a control. Transformants were selected on G418 for 12 days. EGFP-PTP4A3 production was checked by Western blot analysis with the anti-PTP4A3 serum ab26947 (Abcam). The pVNC7 expression vector, encoding the native PTP4A3 and constructed by insertion of the *Eco*RI/*Bam*H1 ORF fragment, was also used to transfect OCM-1 cells (Fig. 3A, OCM-1-VNC7-PTP4A3).

Time-lapse video microscopy

We dispensed 50,000 cells into the wells of six-well plates coated with 50 μg/mL collagen type I (BD Biosciences). Cell migration was monitored by time-lapse video microscopy under bright white light and UV light, with an inverted phase contrast microscope (Leica DM IRB) equipped with an

Published OnlineFirst December 6, 2010; DOI: 10.1158/0008-5472.CAN-10-0605

incubation chamber (37°C, humidified atmosphere containing 5% CO_2), an x–y–z stage controller and a charge-coupled device (CCD) CoolSnap camera (Photometrics). Images were acquired at 4-minute intervals over a 12 hours time period, with the Metamorph software (Molecular Devices). Movies were reconstructed with a plug-in for ImageJ software (http://rsbweb.nih.gov/ij/) developed by F. Cordelière at Institut Curie (Orsay, France). Cells were tracked manually and parameters were calculated with another plug-in also developed by F. Cordelière.

Immunostaining and immunohistochemistry

For the staining of focal adhesions, cells were fixed by incubation for 20 minutes at room temperature in 4% paraformaldehyde and labeled with antibodies against p-FAK (Tyr 397)-R (Santa Cruz Biotechnology) at a dilution 1/500.

Sections (3 μm) were prepared from paraffin-embedded samples and processed for immunohistochemistry by an automated procedure. A polyclonal rabbit antibody, PTP4A3 (P0498 Sigma), was used at a dilution of 1:150. Samples were counterstained with hematoxylin after immunostaining.

Chick embryo metastasis assay

Fertilized chick eggs (EARL Morizeau) were incubated at 38°C, 80% humidity, for 8 days. We then inoculated the chorioallantoid membrane (CAM) with 0.25×10^6 OCM-1-EGFP-PTP4A3, OCM-1-EGFP-PTP4A3(C104S), or OCM-1-EGFP cultured melanoma cells, which were allowed to disseminate during incubation for a further 8 days. The cell lines were introduced in 50 μL of inoculum introduced through a small window in the shell above the CAM generated after the creation of an air pocket between the shell membrane and the CAM.

We assessed the intravasation of melanoma cells from the CAM into the circulation, by the quantitative detection of human *alu* sequences in chick tissue extracts (14). A phenol–chloroform-based protocol was used to extract genomic DNA from dissected femurs treated with SDS, proteinase K and RNaseA. The presence of human *alu* repeats in the chick tissue was assessed by real-time PCR, with primers specific for human *alu* sequences (sense: 5′ CACCTGTAATCCCAGCACTTT 3′, antisense: 5′ CCCAGGCTGGAGTGCAGT 3′, ref. 15), 200 ng of genomic DNA, 3 mM $MgCl_2$, 0.6 μM of each primer, 200 μM dNTPs, 0.625 units of iTaq DNA polymerase (Biorad) and a 1:200 dilution of SYBR Green I dye (iQ SYBR Green Supermix, Biorad). Each PCR was performed in a final volume of 25 μL, with the iCycler iQ™ (Biorad), under the following conditions: 95°C for 3 minutes, followed by 30 cycles of 95°C for 30 s, 65°C for 30 s and 72°C for 30 s.

Amplifiable chick DNA was quantified by amplifying the *GAPDH* gene with the chGAPDH primers (sense: 5′ GAGGAAAGGTCGCCTGGTGGATCG 3′, antisense: 5' GGTGAGGACAAGCAGTGAGGAACG 3′; ref. 14) under the same PCR conditions described for *alu*.

The number of melanoma cells present in each chick femur was estimated by generating a standard curve from a serial dilution of cells. The number of cells present in the femur was then determined by interpolation from the standard curve, for *alu* signals from experimental samples. Data were processed and statistical analysis was carried out with StatView (SAS Institute Inc.) and Microsoft Excel (Microsoft Corporation).

Results

Survival analysis on the 63 patients

Univariate Cox analysis highlighted significant associations between the endpoint (metastasis-free survival) and monosomy 3 ($P = 0.001$), retinal detachment ($P = 0.014$), and epithelioid versus nonepithelioid tumors ($P = 0.027$). In the multivariate Cox *clinical model*, only monosomy 3 ($P = 0.001$) and retinal detachment ($P = 0.023$) were found to be significantly associated with metastasis-free survival (Table 1).

Filtering based on expression values below 3.5 and the removal of half the probe sets (those with the smallest interquartile range), resulted in 37,389 of the initial 54,675 probe sets being discarded. We identified 514 of the remaining 17,286 probe sets as significantly associated with metastasis-free survival. *PTP4A3* was found to be the probe related to metastasis-free survival with the lowest *P* value (corrected $P = 0.003$).

Table 1. Summary of survival analysis

Variables	Clinical model		Genomic model		Clinical and genomic model	
	RR [95% CI]	*P*	RR [95% CI]	*P*	RR [95% CI]	*P*
Monosomy 3						
No	1				1	
Yes	5.93 [2.02 – 17.46]	0.001			3.18 [0.96 – 10.53]	0.058
Retinal detachment						
No	1				1	
Yes	2.74 [1.15 – 6.55]	0.023			2.25 [0.94 – 5.42]	0.069
PTP4A3						
< Median (7)			1		1	
≥ Median (7)			4.39 [2.09 – 9.22]	<0.001	3.33 [1.29 – 8.58]	0.013

Abbreviation: RR, relative risk.

Published OnlineFirst December 6, 2010; DOI: 10.1158/0008-5472.CAN-10-0605

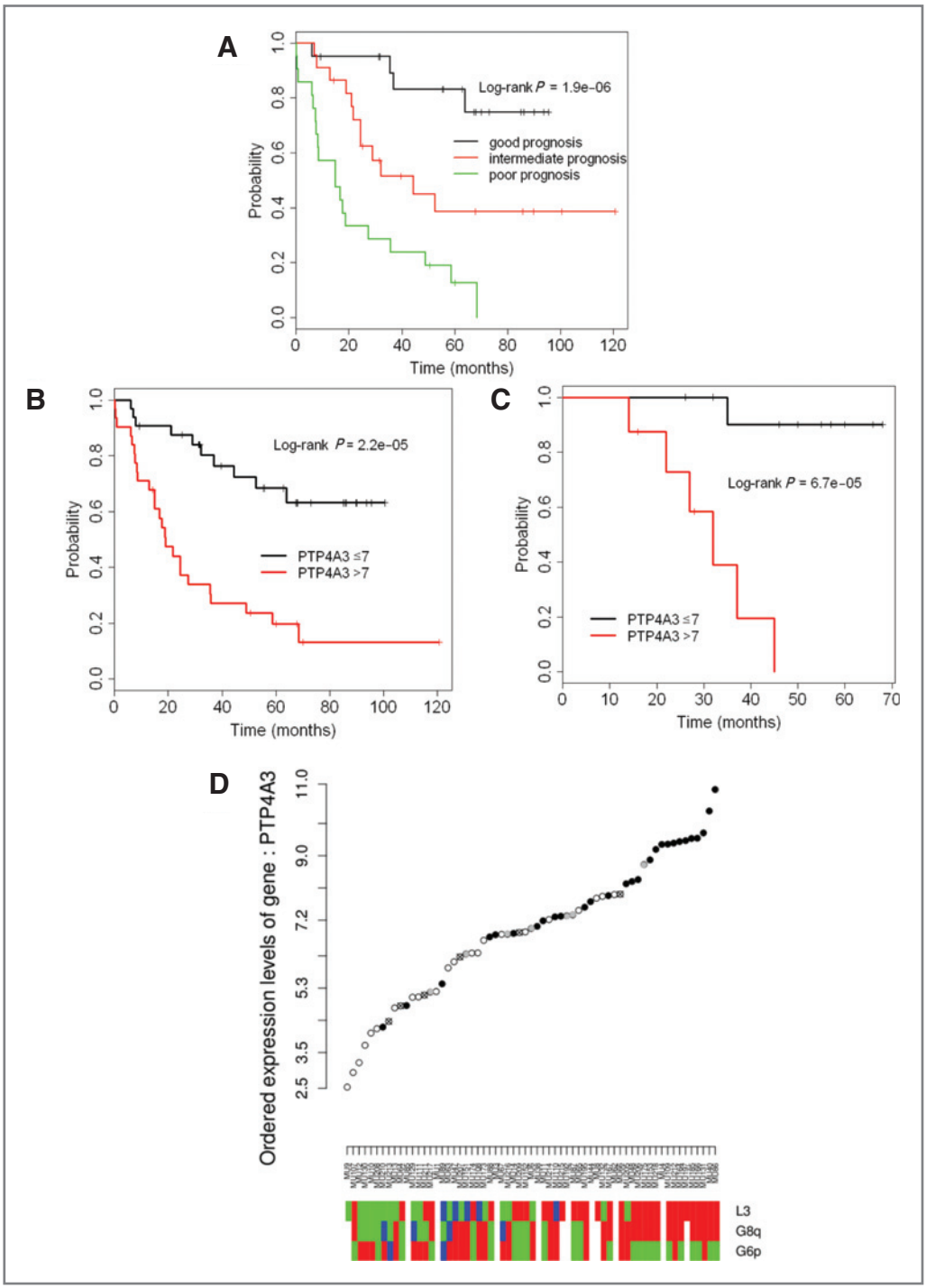

Figure 1. Kaplan–Meier analysis and *PTP4A3* levels. A–C, Kaplan–Meier plots of metastasis-free survival. A, identification of groups of patients with different prognoses based on the score predicted by the *clinical–genomic model* (monosomy 3, retinal detachment, and PTP4A4 as a binary variable). B, identification of two groups of patients with different prognoses based on the predicted score from the *genomic model* (PTP4A4 as a binary variable). C, validation of the median as a threshold in the *genomic model* for the identification of two different groups, for an external data set (21 primary tumors) (3). D, PTP4A3-ordered expression level ($\log_2$) on 63 primary tumors. Black points, metastatic tumors. White points, nonmetastatic tumors. Gray points, tumors metastasizing late (after 36 months, considered *meta0* in our analysis). Crossed points, tumors with less than 36 months of follow-up. The heatmap below shows known chromosome alterations. L3, loss of chromosome 3; G8q, gain of the 8q region, and G6p, gain of the 6p region. Green, no alteration. Red, alteration. Blue, partial alteration. White, not available data about chromosomal alterations in these tumors.

Published OnlineFirst December 6, 2010; DOI: 10.1158/0008-5472.CAN-10-0605

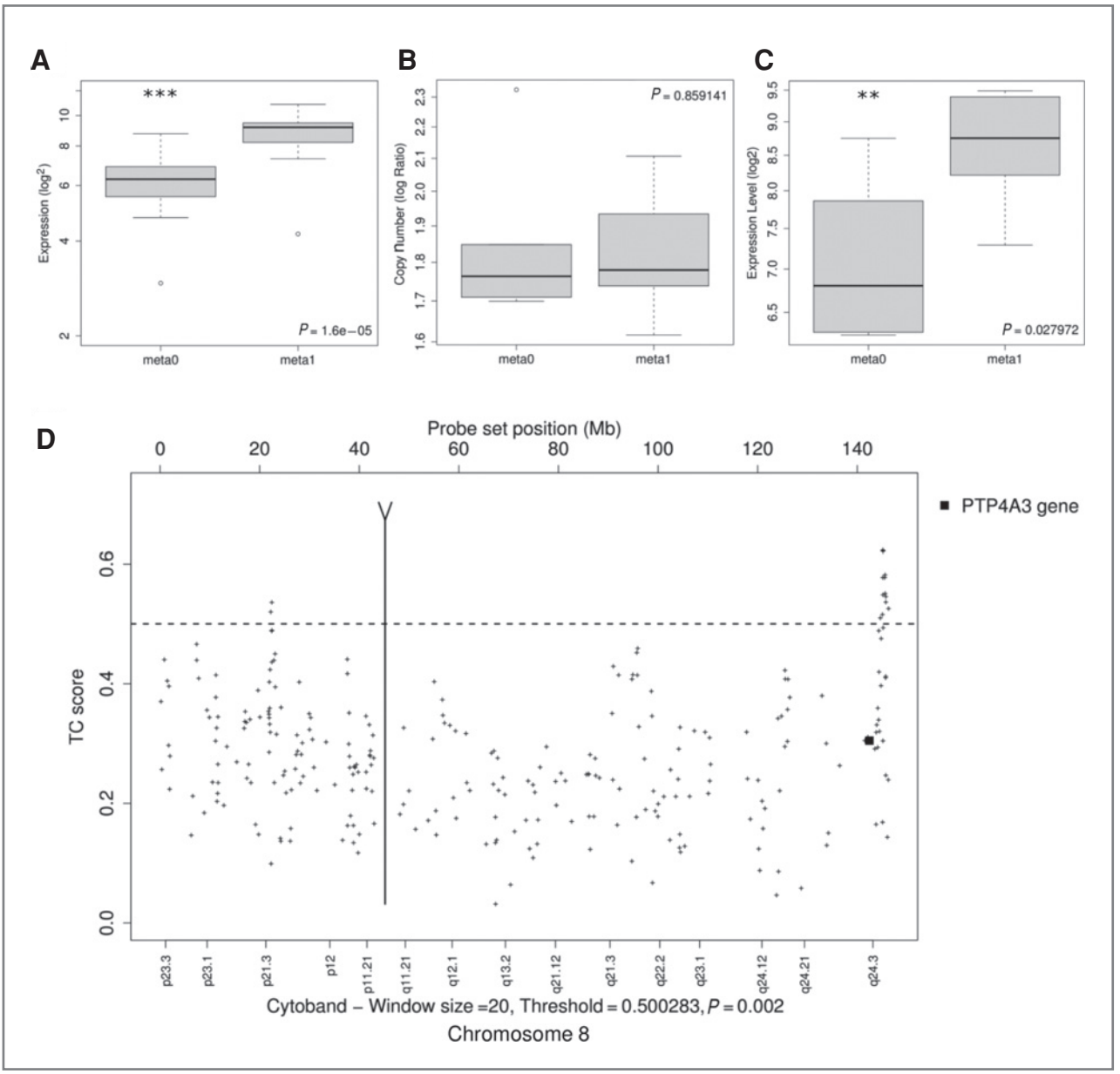

Figure 2. PTP4A3 is not a chromosome 8 passenger gene. A–C, boxplots representing the distribution of $\log_2$ expression values (A, C) or log-ratio DNA copy number for *PTP4A3* (B). *P* values were obtained for a Wilcoxon rank-sum test. A, tumors with 8q region overrepresentation ($N = 32$, *meta0* = 15, *meta1* = 17). B and C, tumors displaying homogeneous overrepresentation of 8q ($N = 15$, *meta0* = 5, *meta1* = 10). ***, $P < 10^{-3}$, **, $P < 5 \times 10^{-2}$. D, transcriptome correlation map for tumors with 8q region overrepresentation ($N = 32$). The TC score indicates the significance of the correlation between the expression of a given gene and that of its neighbors (20 neighbors in this case).

PTP4A3 treated as a binary variable (median expression level, equal to 7, used as a threshold) was also strongly associated with metastasis-free survival ($P < 0.001$) and remained significant when the multivariate Cox model was adjusted for the parameters of the *clinical model* ($P = 0.013$, Table 1).

The scores provided by the *clinical and genomic* models made it possible to define three significantly different groups with a "good," "intermediate," and "poor" prognosis (Fig. 1A) of developing metastases (log-rank test, $P = 1.9 \times 10^{-6}$). As shown in Figure 1B, the scores provided by the *genomic model* (with only *PTP4A3* as a binary variable) identified two groups of patients with significantly different risks of metastasis development (log-rank test, $P = 2.2 \times 10^{-5}$). Similar significant results were obtained with an external data set (ref. 3; Fig. 1C; log-rank test, $P = 6.7 \times 10^{-5}$).

Differential expression of *PTP4A3* is not linked to the overrepresentation of chromosome 8

An analysis of differential expression between 29 *meta0* and 28 *meta1* tumors identified 983 probe sets as differentially

Published OnlineFirst December 6, 2010; DOI: 10.1158/0008-5472.CAN-10-0605

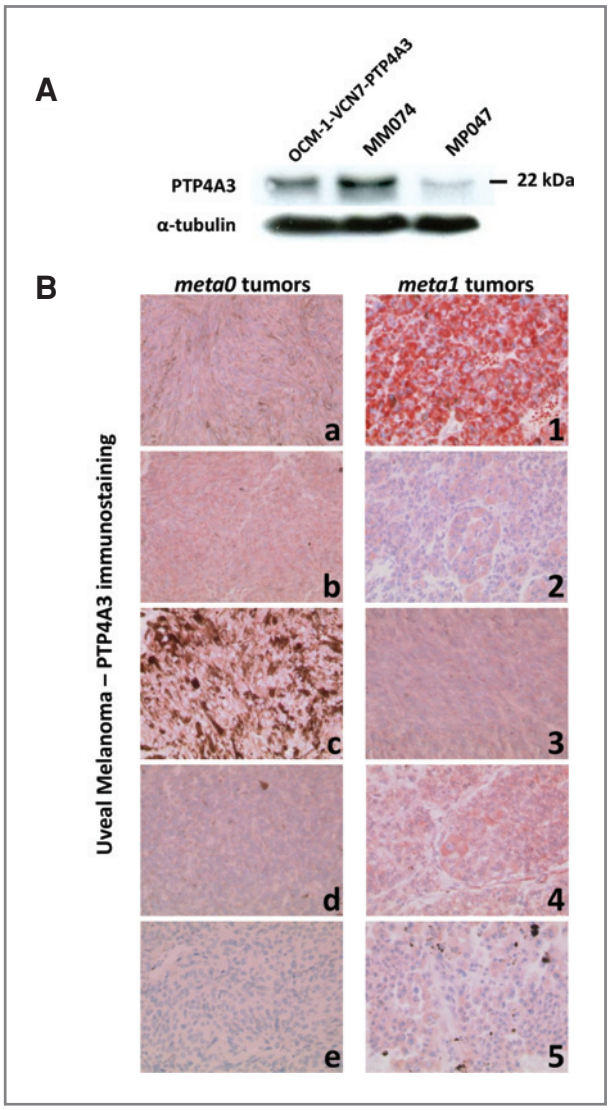

Figure 3. Immunodetection of PTP4A3. A, Western blot analysis of the specificity of the anti-PTP4A3 antibody. A specific band of about 22 kDa was detected in OCM-1 cell lines overproducing PTP4A3. An identical specific band, the intensity of which was correlated with the RNA level obtained by RT-qPCR (data not shown), was observed in tumor extracts of mouse xenografts (MM074, MP047). B, immunohistochemistry: examples of *meta0* and *meta1* primary tumors with weak (*meta0* tumors, a–e) and strong PTP4A3 immunostaining (*meta1* tumors, 1–5), respectively (original magnification × 200). Positive staining appears in red and nuclei were counterstained with hematoxylin.

expressed, with an FDR of 5%. *PTP4A3* was one of the most strongly differentially expressed genes ($P < 10^{-5}$).

PTP4A3 is located in 8q24.3, a region significantly overrepresented in metastatic tumors (2). High levels of *PTP4A3* mRNA may therefore simply be a consequence of chromosome overrepresentation. However, not all uveal melanomas with 8q overrepresentation overexpress this gene (Fig. 1D). We therefore investigated a subgroup of 32 tumors with 8q overrepresentation and looked for significant differences in *PTP4A3* RNA levels between *meta0* and *meta1* tumors in this subgroup (Fig. 2A). *PTP4A3* was significantly more strongly expressed in the *meta1* group ($P < 0.01$), but *PTP4A3* gene copy number level varied in these tumors. We performed the same analysis on a subgroup of 15 tumors (5 *meta0*, 10 *meta1*) with identical DNA copy numbers for this gene ($P = 0.86$, Fig. 2B). *PTP4A3* was again found to be significantly more strongly expressed in *meta1* than in *meta0* tumors in this subgroup ($P = 0.028$, Fig. 2C). Thus, *PTP4A3* overexpression is not simply a consequence of chromosome overrepresentation.

We investigated whether *PTP4A3* was coexpressed with other genes from the 8q region by studying the correlation between the expression of *PTP4A3* expression and that of its nearest neighbors in the same orientation (similar results were obtained without this selection of DNA orientation). TCM analysis (12) showed that the expression of *PTP4A3* was not correlated with that of its neighbors (Fig. 2D). Indeed, *PTP4A3* was the only gene in this region differentially expressed between *meta0* and *meta1* tumors at the chosen level of significance (data not shown). Thus, the overexpression of *PTP4A3* in *meta1* tumors cannot be accounted for by *PTP4A3* acting as an 8q passenger gene.

As chromosome 6p overrepresentation is associated with a lower risk of metastasis development (in our 45 tumors, $P = 0.0078$) and of cutaneous melanoma (16), we separated tumors displaying chromosome 8q overrepresentation ($N = 32$) from those with a normal chromosome 6 ($N = 14$) and those with an overrepresented 6p ($N = 18$). In the subgroup of tumors with 6p overrepresentation, *PTP4A3* expression levels were significantly lower ($P = 0.01$) than in tumors bearing normal amounts of 6p. In tumors in which both 6p and 8q were overrepresented, *PTP4A3* expression level was not a significant marker of *meta1* tumors ($N = 18$, with *meta0* = 12 and *meta1* = 6; $P = 0.1$). This suggests that the protective effect of chromosome 6p overrepresentation against melanoma metastasis may be in part linked to a reduced *PTP4A3* RNA level.

PTP4A3 is overexpressed in *meta1* tumors

We investigated whether protein levels were correlated with mRNA levels for PTP4A3 in uveal melanoma tumors, we performed immunodetection of this protein in sections from *meta0* and *meta1* tumors. A Western blot analysis of OCM-1 cells displaying PTP4A3 upregulation was carried out, to validate the antibody against PTP4A3 used for immunohistochemistry. OCM-1 cells were transiently transfected to overexpress *PTP4A3*. We then subjected 20 μg of cell lysate/lane to SDS-PAGE and Western blotting with the PTP4A3 antibody. A specific band of about 22 kDa was detected in OCM-1 cells overexpressing *PTP4A3* (Fig. 3A). Under the experimental conditions used, endogenous PTP4A3 protein levels in OCM-1 cells were below the detection limit. We then used tumor cell lysates obtained from mouse xenografts (17) with high (MM074) or low (MP047) PTP4A3 RNA levels, as determined by RT-qPCR (data not shown and Fig. 3A). Sections of these tumors were used to set up the immunodetection conditions. The results obtained with human tumor sections

Published OnlineFirst December 6, 2010; DOI: 10.1158/0008-5472.CAN-10-0605

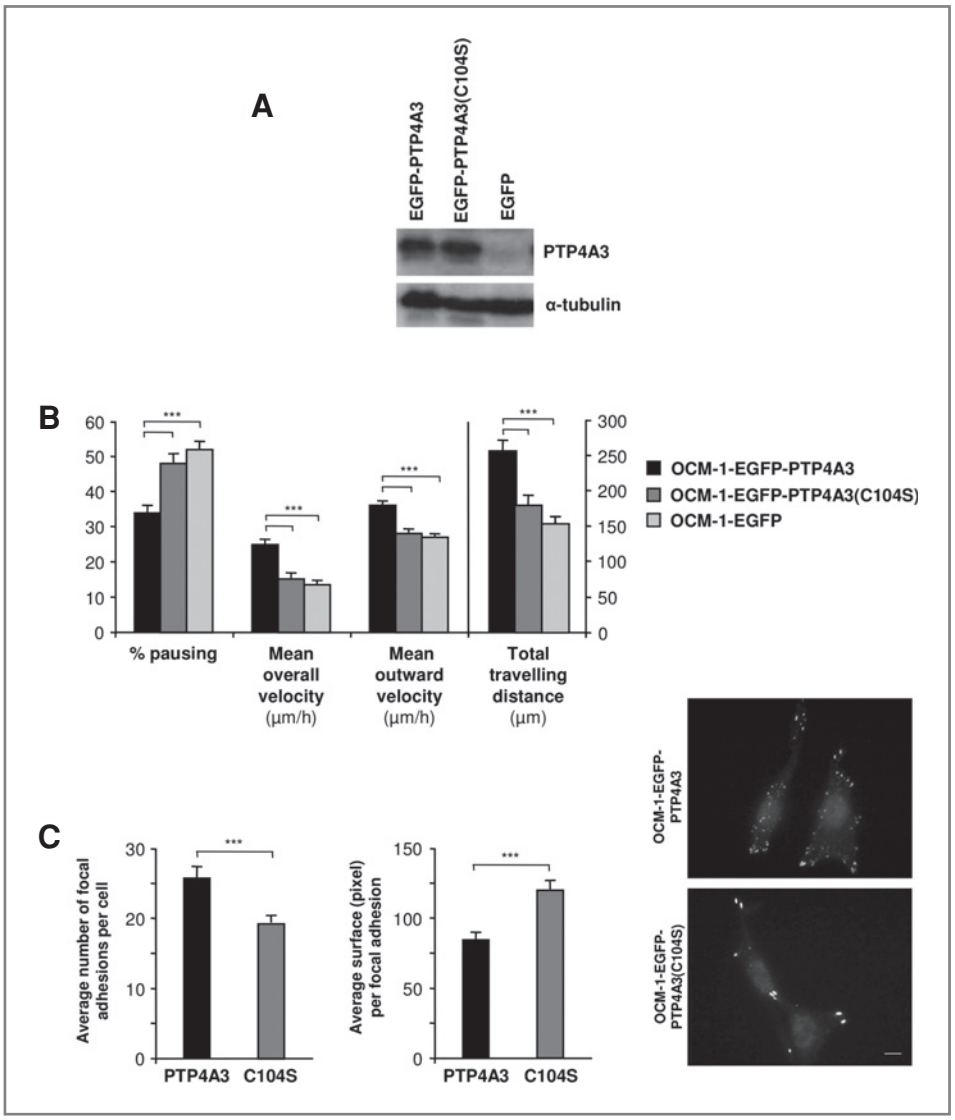

Figure 4. Involvement of PTP4A3 in uveal melanoma cell migration. A, establishment of OCM-1 cell lines producing EGFP-PTP4A3, EGFP-PTP4A3(C104S), or EGFP. Western blot analysis of cell lysates. B, the overproduction of PTP4A3 promotes the migration of human uveal melanoma cells on collagen I matrix. Migratory characteristics were assessed by determining four parameters. Histograms indicate the mean values of two independent experiments, performed in duplicate. Number of tracked cells: OCM-1-EGFP-PTP4A3 = 51, OCM-1-PTP4A3(C104S) = 39, and OCM-1-EGFP = 46. Error bars show the coefficient of variation; ***, $P < 1.2 \times 10^{-5}$. Similar results were obtained with two other independent clones for each construct (not shown). C, histograms showed the number (left) and the surface area (right) of phospho-PTK2–labeled focal adhesions in the cells described in Figure 4A. Images of representative phospho-PTK2 staining for focal adhesions are presented for the cells indicated. Protein distribution was determined by three-dimensional fluorescence microscopy on fixed cells. Two cells were included. Bar, 10 μm.

are shown in Figure 3B, positive staining appears in red and nuclei were counterstained with hematoxylin. Left column, PTP4A3 negative *meta0* tumors (e.g., in panel a *PTP4A3* $\log_2$ expression: 4.67) and right column PTP4A3 positive *meta1* tumors (e.g., in panel 1, *PTP4A3* $\log_2$ expression: 10.41).

PTP4A3 overexpression increases migration in uveal melanoma cells

PTP4A3 is known to promote cell migration and invasion in several types of cancer cell *in vitro* and *in vivo* (18–22). OCM-1 uveal melanoma cell lines stably producing wild-type PTP4A3 or the catalytic mutant C104S (ref. 19, Fig. 4A) were established. As PTP4A3 has been reported to interact with integrin α1 and to regulate integrin β1 phosphorylation (23), we performed random migration assays, in which migration on collagen I matrix was compared with that on uncoated tissue culture dishes. Time-lapse video microscopy experiments revealed that OCM-1 cells producing the wild-type PTP4A3 migrated faster, paused for shorter periods and traveled further on collagen I matrix than did cells producing the mutant protein or EGFP alone (Fig. 4B and videos 1–3 in Supplementary data). OCM-1 cells producing the wild-type PTP4A3 had a significantly larger number of focal adhesions covering a significantly smaller surface area than cells producing the mutant form of the phosphatase (Fig. 4C).

PTP4A3 overproduction increases the invasiveness of uveal melanoma cell lines

The chick embryo can be used as a naturally immunodeficient host capable of sustaining graft tissues and cells without species-specific restrictions. The use of these embryos makes it possible to carry out a comprehensive analysis of the dissemination of cancer cells, including tumor cell

Published OnlineFirst December 6, 2010; DOI: 10.1158/0008-5472.CAN-10-0605

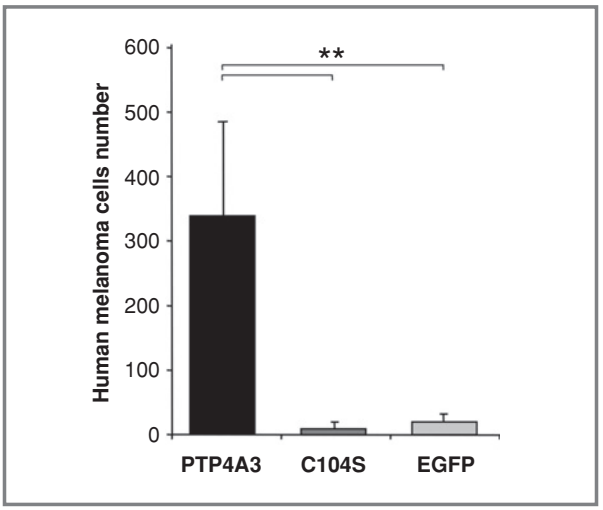

Figure 5. Involvement of PTP4A3 in uveal melanoma cell invasiveness. Quantitative analysis of invasiveness in the chick embryo, using OCM-1 clones producing EGFP-PTP4A3, EGFP- PTP4A3(C104S), or EGFP. Eight days after 0.25×10^6 cells were used to inoculate the CAM of 8-day-old embryos, femurs were isolated. The DNA extracted (200 ng) was subjected to quantitative real-time PCR with human *alu* and chicken *GAPDH* primers. The number of cells present was calculated from the standard curve. Similar data were obtained in two independent experiments. Number of inoculated embryos: OCM-1-EGFP-PTP4A3 = 5, OCM-1-EGFP-PTP4A3 (C104S) = 8, and OCM-1-EGFP = 3. Errors bars indicate the coefficient of variation; $^{**}P = 0.01$.

intravasation in a model of spontaneous metastasis (24). Uveal melanoma OCM-1 cell lines producing EGFP-PTP4A3, EGFP-PTP4A3(C104S), or EGFP were grafted *in ovo*. One week after inoculation, femurs were dissected and DNA extracted for qPCR experiments with human *alu*-specific oligonucleotides. High levels of colonization occurred only in OCM-1 cells expressing *PTP4A3* (Fig. 5).

Discussion

Our study showed that a new predictive gene, *PTP4A3*, is differentially expressed between *meta0* and *meta1* primary tumors and strongly associated with the occurrence of metastasis in uveal melanoma. *PTP4A3* is located on 8q, but its overexpression in *meta1* tumors was not due to 8q overrepresentation. Moreover, *PTP4A3* was no longer linked to metastasis risk in the presence of chromosome 6p gain, potentially accounting for the protective effect of 6p overrepresentation. Our analysis was carried out on large tumors only, as only such tumors are obtained by enucleation. Our findings may not, therefore, be applicable to all uveal melanomas and tumors with chromosome 3 monosomy were probably overrepresented in our sample. The role of *PTP4A3* in smaller tumors remains to be studied. The immunodetection of PTP4A3 in tumor sections demonstrated a positive correlation between RNA and protein levels. Recently, PCBP1 a RNA-binding protein has been demonstrated as able to suppress the translation of PTP4A3 (25). Because few *meta*0 tumors expressed high levels of *PTP4A3* mRNA (Fig. 1D), a correlation between PTP4A3 and PCBP1 immunostaining and metastasis occurrence remains to be performed with a large sample of tumors.

Uveal melanoma cell lines overexpressing *PTP4A3* migrate faster, spend less time pausing and travel further than cells producing the C104S phosphatase mutant. They also have a larger number of focal adhesions covering a smaller surface area, as shown by phospho-PTK2 staining. The formation and remodeling of focal contacts is a dynamic process regulated by protein tyrosine kinases and small GTPases of the Rho family (26) and modulated by PTP4A3. In our transcriptome analysis, *PTK2* expression was found to be correlated with *PTP4A3* RNA level ($R = 0.71$, $P < 0.001$). Invasion assays with other cancer cells indicated that PTP4A3 was involved in the invasion of these cells *in vivo* (18, 22, 27). In the CAM assay, uveal melanoma cell lines producing PTP4A3 were invasive and found in the femur of injected embryos, whereas those producing the mutant phosphatase were not. Thus, in addition to increasing cell migration, PTP4A3 may be involved in the regulation of protease-encoding genes. *PTP4A3* expression was correlated with the expression of proteases (*ADAM10, ADAM23, CAPN2, IDE, HTRA1*) in our sample tumors, and inversely correlated with *TIMP3* protease inhibitor levels ($R = -0.57$, $P < 0.001$). MMPs and TIMPs are positive and negative regulators, respectively, of tissue remodeling and tumor progression (28). A direct role for PTP4A3 in the regulation of protease-encoding genes is suggested by the observation that *ADAM23* is significantly more strongly expressed in OCM-1 cells expressing EGFP-PTP4A3 than in OCM-1-EGFP-PTP4A3(C104S), or OCM-1-EGFP cells (unpublished data).

Our results indicate that *PTP4A3* may be more than a simple marker of prognosis in terms of metastasis. Instead, it may play a causal role in the development of metastases in uveal melanoma. *PTP4A3* is therefore a good candidate target for treatment strategies.

Disclosure of Potential Conflicts of Interest

No potential conflicts of interest were disclosed.

Acknowledgments

We would like to thank Laetitia Marisa, Pascale Trouillet, André Nicolas, Anna Almeida, Fariba Nemati, Pierre Gestraud, and Pierre Neuvial for their contributions to this work.

Grant Support

This work was supported by grants from the Department of Translational Research, Institut Curie, CNRS, INSERM, Cancéropole Ile-de-France, Association pour la Recherche sur le Cancer, Retina France, and Ligue Nationale Contre le Cancer.

The costs of publication of this article were defrayed in part by the payment of page charges. This article must therefore be hereby marked *advertisement* in accordance with 18 U.S.C. Section 1734 solely to indicate this fact.

Received February 18, 2010; Revised November 4, 2010; accepted November 5, 2010; published OnlineFirst December 6, 2010.

Published OnlineFirst December 6, 2010; DOI: 10.1158/0008-5472.CAN-10-0605

References

1. Gargoudas ES, Egan KM, Seddon JM, Glynn RJ, Walsh SM, Finn SM, et al. Survival of patients with metastases from uveal melanoma. Ophthalmology 1991;98:383–9.
2. Trolet J, Hupé P, Huon I, Lebigot I, Decraene C, Delattre O, et al. Genomic profiling and identification of high risk uveal melanoma by array-CGH analysis of primary tumors and liver metastases. Invest Ophthalmol Vis Sci 2009;50:2572–80.
3. Onken MD, Worley LA, Ehlers JP, Harbour JW. Gene expression profiling in uveal melanoma reveals two molecular classes and predicts metastatic death. Cancer Res 2004;64:7205–9.
4. Onken MD, Ehlers JP, Worley LA, Makita J, Yokota Y, Harbour JW. Functional gene expression analysis uncovers phenotypic switch in aggressive uveal melanomas. Cancer Res 2006;66:4602–9.
5. Petrausch U, Martus P, Tönnies H, Bechrakis NE, Lenze D, Wansel S, et al. Significance of gene expression analysis in uveal melanoma in comparison to standard risk factors for risk assessment of subsequent metastases. Eye 2008; 22:997–1007.
6. Onken MD, Worley LA, Tuscan MD, Harbour JW. An accurate, clinically feasible multi-gene expression assay for predicting metastasis in uveal melanoma. J Mol Diag 2010;12:461–8.
7. R Development Core Team (2009). R: A Language and Environment for Statistical Computing. Vienna, Austria:R Foundation for Statistical Computing. ISBN 3-900051-07-0. Available from:http://www.R-project.org.
8. Gentleman RC, Carey VJ, Bates DM, Bolstad B, Dettling M, Dudoit S, et al. Bioconductor: open software development for computational biology and bioinformatics. Genome Biol 2004;5:R80–R80.16.
9. Wu Z, Irizarry RA, Gentleman R, Martinez-Murillo F, Spencer F. A model-based background adjustment for oligonucleotide expression arrays. J Am Stat Assoc 2004;99:909–18.
10. Benjamini Y, Hochberg Y. Controlling the false discovery rate: a practical and powerful approach to multiple testing. J Roy Stat Soc Ser 1995;B57:289–300.
11. Tusher VG, Tibshirani R, Chu G. Significance analysis of microarrays applied to the ionizing radiation response. Proc Natl Acad Sci U S A 2001;98:5116–21.
12. Reyal F, Stransky N, Bernard-Pierrot I, Vincent-Salomon A, de Rycke Y, Elvin P, et al. Visualizing chromosomes as transcriptome correlation maps: evidence of chromosomal domains containing co-expressed genes—a study of 130 invasive ductal breast carcinomas.Cancer Res 2005;65:1376–83.
13. Kan-Mitchell J, Mitchell MS, Rao N, Liggett PE. Characterization of uveal melanoma cell lines that grow as xenografts in rabbit eyes. Invest Ophthalmol Vis Sci 1989;30:829–34.
14. Zijlstra A, Mellor R, Panzarella G, Aimes RT, Hooper JD, Marchenko ND, et al. A quantitative analysis of rate-limiting steps in the metastatic cascade using human-specific real-time polymerase chain reaction. Cancer Res 2002;62:7083–92.
15. Schneider T, Osl F, Friess T, Stockinger H, Scheuer VW. Quantification of human Alu sequences by real-time PCR—an improved method to measure therapeutic efficacy of anti-metastatic drugs in human xenotransplants. Clin Exp Metastasis 2002;19:571–82.
16. Goldberg SF, Miele ME, Hatta N, Takata M, Paquette-Straub C, Freedman LP, et al. Melanoma metastasis suppression by chromosome 6: evidence for a pathway regulated by CRSP3 and TXNIP. Cancer Res 2003;63:432–40.
17. Nemati F, Sastre-Garau X, Laurent C, Couturier J, Mariani P, Desjardins L, et al. Establishment and characterization of a panel of human uveal melanoma xenografts derived from primary and/or metastatic tumors. Clin Cancer Res 2010;16:2352–62.
18. Wu X, Zeng H, Zhang X, Zhao Y, Sha H, Ge X, et al. Phosphatase of regenerating liver-3 promotes motility and metastasis of mouse melanoma cells. Am J Pathol 2004;164:2039–54.
19. Wang H, Quah YS, Dong JM, Manser E, Tang JP, Zeng Q. PRL-3 down-regulates PTEN expression and signals through PI3K to promote epithelial-mesenchymal transition. Cancer Res 2007;67:2922–26.
20. Liang F, Liang J, Wang WQ, Sun JP, Udho E, Zhang ZY. PRL3 promotes cell invasion and proliferation by down-regulation of Csk leading to Src activation. J Biol Chem 2007;282:5413–9.
21. Saha S, Bardelli A, Buckhaults P, Velculescu VE, Rago C, St Croix B, et al. A phosphatase associated with metastasis of colorectal cancer. Science 2001;294:1343–6.
22. Miskad UA, Semba S, Kato H, Yokozaki H. Expression of PRL-3 phosphatase in human gastric carcinomas: close correlation with invasion and metastasis. Pathobiology 2004;71:176–84.
23. Peng L, Jin G, Wang L, Guo J, Meng L, Shou C. Identification of integrin alpha1 as an interacting protein of protein tyrosine phosphatase PTP4A3. Biochem Biophys Res Commun 2006;342:179–83.
24. Deryugina EI, Quigley JP. Chick embryo chorioallantoic membrane model systems to study and visualize human tumor cell metastasis. Histochem Cell Biol 2008;130:1119–30.
25. Wang H, Vardy LA, Tan CP, Loo JM, Guo K, Li J, et al. PCBP1 suppresses the translation of metastasis-associated PRL-3 phosphatase. Cancer Cell 2010 ;18:52–62.
26. Parsons JT, Martin KH, Slack JK, Taylor JM, Weed SA. Focal adhesion kinase: a regulator of focal adhesion dynamics and cell movement. Oncogene 2000;19:5606–13.
27. Li Z, Zhan W, Wang Z, Zhu B, He Y, Peng J, et al. Inhibition of PRL-3 gene expression in gastric cancer cell line SGC7901 via microRNA suppressed reduces peritoneal metastasis. Biochem Biophys Res Commun 2006; 348:229–37.
28. Bourboulia D, Stetler-Stevenson WG. Matrix metalloproteinases (MMPs) and tissue inhibitors of metalloproteinases (TIMPs): positive and negative regulators in tumor cell adhesion. Semin Cancer Biol. 2010;20:161–8.

Cancer Research
The Journal of Cancer Research (1916–1930) | The American Journal of Cancer (1931–1940)

AACR American Association for Cancer Research

High PTP4A3 Phosphatase Expression Correlates with Metastatic Risk in Uveal Melanoma Patients

Cécile Laurent, Fabien Valet, Nathalie Planque, et al.

Cancer Res 2011;71:666-674. Published OnlineFirst December 6, 2010.